Journal of Molecular Graphics and Modelling 44 (2013) 81–90

Contents lists available at ScienceDirect

Journal of Molecular Graphics and Modelling

journal homepage: www.elsevier.com/locate/JMGM

Complex between *Human* RNase HI and the phosphonate-DNA/RNA duplex: Molecular dynamics study

Kamil Maláč, Ivan Barvík*

Charles University, Faculty of Mathematics and Physics, Institute of Physics, Ke Karlovu 5, Prague 2 121 16, Czech Republic

ARTICLE INFO

Article history:
Received 7 October 2012
Received in revised form 30 April 2013
Accepted 5 May 2013
Available online 17 May 2013

Keywords:
RNase H
Antisense oligonucleotides
Argonaute
RNAi
Phosphonate
Molecular dynamics
ACEMD

ABSTRACT

Our 200 ns MD simulations show that even fully modified oligonucleotides bearing the 3′-O-P-CH_2-O-5′ (but not 3′-O-CH_2-P-O-5′) phosphonate linkages can be successfully attached to the surface of *Human* RNase H. It enables to explain that oligonucleotides consisting of the alternating 3′-O-P-CH_2-O-5′ phosphonate and phosphodiester linkages are capable to elicit the RNase H activity (while the 3′-O-CH_2-P-O-5′ phosphonates are completely inactive). Stability of the binuclear active site of *Human* RNase H was achieved using the one-atom model for Mg^{2+} in conjunction with a polarized phosphate group of the scissile bond, which is wedged between both magnesium ions. The reference MD simulation (lasting for 1000 ns), which was produced using a well-established seven-point (with dummy atoms) model for Mg^{2+} led to essentially the same results. The MD run (lasting for 500 ns) produced for the *Thermus thermophilus* Argonaute enzyme shows the transferability of our approach for the stabilization of a binuclear active site. Glu512 was bound in the *T. thermophilus* Argonaute active site to the 2′-OH of the nucleotide adjacent to the scissile phosphate and one of the two active-site divalent metal ions in exactly the same way as Glu186 in *Human* RNase H. Glu512 thus completes the catalytic tetrad of Argonaute.

© 2013 Elsevier Inc. All rights reserved.

1. Introduction

So called “antisense” oligonucleotides represent a perspective approach in chemotherapy, promising to inhibit selectively unwanted gene expression by creation of a helical complex with target mRNA (carrying “sense” genetic information) [1–8]. Several antisense oligonucleotide constructs, selected from many hundreds, were able to proceed to clinical trials and use [9,10]. If hybridization between the target mRNA and the exogenous nucleotide sequence occurs, a duplex is created, which forms a jam that prevents the ribosomal complex from reading along the message. If the ribosomal complex cannot read the message, the appropriate tRNAs are not assembled and the encoded peptide is not made. However, RNA–DNA duplexes can be unwound by a variety of repair/editing enzymes. In addition, the ribosomal complex itself has an unwindase activity that likely permits reading of the complexly fold mRNA [7]. Fortunately, some deoxyoligonucleotides support the binding of ribonuclease H (RNase H) at sites of RNA–DNA duplex formation. Such binding is thought to be an important effector of antisense actions because once bound, RNase H, a ubiquitous nuclear enzyme required for DNA synthesis, functions as an endonuclease that recognizes and cleaves the RNA in the duplex. Once initiated, destruction of the message by cleavage is assured. Of significant interest also is the fact that the DNA comprising in the duplex is undamaged by the enzymatic attack. Therefore, it is free to hybridize with multiple RNA molecules, leading their destruction in a catalytic manner [7].

RNA interference (RNAi, discovered in 1998 [11–13]) is a eukaryotic-specific gene-silencing pathway triggered by double-stranded RNA (dsRNA) [14]. In this pathway, the RNase III enzyme Dicer first cleaves the dsRNA trigger into small interfering RNAs (siRNAs). The siRNA duplex is incorporated into the effector protein Argonaute (AGO) – analogous to RNase H, at which point one of the strands is cleaved. After the cleaved strand is discarded, the resulting ribonucleoprotein complex uses the remaining siRNA strand to specify interactions with target RNAs. If sequence complementarity between quide and target strands is extensive, AGO again catalyzes cleavage, resulting in ‘slicing’ of the target RNA [14].

The oligonucleotides with natural chemical composition, the first candidates for the “antisense/siRNA” drugs, have been, however, found as unsuitable for in vivo applications because of their insufficient resistance against nucleases. Oligonucleotides consisting of both the 3′-O-P-CH_2-O-5′ and phosphodiester linkages are capable to elicit RNase H activity [15]. The oligonucleotides with either the 3′-O-P-CH_2-O-5′ or 3′-O-CH_2-P-O-5′ linkage has been investigated by means of molecular dynamics (MD) simulations [16–18]. Binding of DNA (and of its phosphonate analogs) toward EC RNase H was modeled [19]. Plausibility of this model

* Corresponding author. Tel.: +420 221 911 450; fax: +420 224 922 797.
E-mail address: ibarvik@karlov.mff.cuni.cz (I. Barvík).

1093-3263/$ – see front matter © 2013 Elsevier Inc. All rights reserved.
http://dx.doi.org/10.1016/j.jmgm.2013.05.004

was confirmed later by crystal structures of HS RNase H [20]. There are many analogous residues (EC/HS RNase H – Trp85/Tr225, Trp81/Trp221, Thr43/Thr181, etc.) bound to nucleic acids with truly perfect compliance at the atomic level. Further, impacts of phosphonate internucleotide linkages placed in various positions along DNA on its binding toward EC RNase H were investigated in past by means of short (1.5 ns) MD simulations [19].

Here, graphics processing units (GPUs) were used to extend such MD trajectories up to 200 ns. The ability of 3′-O-P-CH_2-O-5′ and 3′-O-CH_2-P-O-5′ phosphonate oligonucleotides to bind toward HS RNase H was studied in detail. Stability of the binuclear active site of HS RNase H was achieved using the one-atom model for Mg^{2+} in conjunction with a polarized phosphate group of the scissile bond (wedged between both magnesium ions). The reference MD simulation (lasting for 1000 ns and produced using a well-established seven-point model for Mg^{2+} [21]) led to essentially the same results. In future, we intend to compare MD trajectories gained in this study with those carried out for differently modified DNA chains.

RNase H forms its active site during initial folding. This active site is well-suited to its role in nonspecifically cleaving RNA–DNA hybrids. In contrast, proper function of AGO requires high specificity, therefore a conformational change occurs to form its active site [14]. Although the PIWI domain of AGO has an RNase H fold, only a conserved 'DDX' catalytic triad (where 'X' is generally Asp or His) had been recognized in AGOs with slicer activity. Nevertheless, the recent crystal structure of *Kluyveromyces polysporus* Argonaute (KpAGO) [14] uncovered a hydrogen-bond network that stabilizes an expanded and repositioned loop, which inserts an invariant glutamate into the catalytic pocket. The structures of ternary *Thermus thermophilus* Argonaute (TtAGO) complexes in the glutamate plugged-in conformation show the position of loop L2 in the context of guide and target strands [22]. TtAGO loop L2 interacts with the guide DNA at positions 11–15. Moreover, the carboxyl group of the glutamate finger Glu512 approaches both the 2′-OH of the nucleotide adjacent to the scissile phosphate and one of the two active-site divalent metal ions, which indicates that the glutamate finger might act as a catalytic residue [14,22]. The putative DEDD catalytic tetrads in conformations of both TtAGO and KpAGO are nearly isosteric with the RNase H DEDD tetrad. Moreover, only mutation of KpAGO Glu1013 (homologous to TtAGO Glu512) abrogated RNAi to the extent observed for mutation of KpAGO Asp1046, a previously identified active-site residue [14]. Thus, it was proposed that the glutamate finger constitutes the second residue of a universally conserved RNase H-like DEDX catalytic tetrad at the active site of slicing AGOs [14].

The MD run (lasting for 500 ns) produced here for TtAGO shows the transferability of our approach for the stabilization of a binuclear active site. Glu512 was bound in the TtAGO active site to the 2′-OH of the nucleotide adjacent to the scissile phosphate and one of the two active-site divalent metal ions in exactly the same way as Glu186 in HS RNase H. Glu512 thus completes the catalytic tetrad of TtAGO.

2. Methods

The model of HS RNase H complexed with a phosphonate-DNA:RNA hybrid was constructed using the recent crystal structure [20] (Protein Data Bank entry 2QKK). Base pairs not participating in the DNA:RNA binding toward the enzyme were omitted from the simulated system. Three modified internucleotide linkages (either the 3′-O-P-**CH_2**-O-5′/**3pc5** or 3′-O-**CH_2**-P-O-5′/**3pc5** type) were incorporated into the 3′-end of DNA (i.e. 3′-G-**3pc5**-C-**3pc5**-T-**3pc5**-G-T-G-G-A-5′ or 3′-G-**3cp5**-C-**3cp5**-T-**3cp5**-G-T-G-G-A-5′). Both simulated systems (HS RNase H + 3pc5-DNA:RNA and HS RNase H + 3cp5-DNA:RNA) were surrounded by TIP3P [23] water molecules which extended to a distance of approximately 10 Å (in each direction) from the enzyme-nucleic acids atoms. This gives a periodic box size of ~82 Å, ~81 Å, ~61 Å for a simulated system consisting of 39,577 atoms. Similarly, the TtAGO enzyme [22] (Protein Data Bank entry 3HVR) was surrounded by TIP3P water molecules (periodic box size ~117 Å, ~106 Å, ~87 Å, 88,603 atoms). New *.inpcrd (initial coordinates) and *.prmtop (molecular topology, force field etc.) files for the whole simulated system, were created by means of the TLEAP module (the AMBER software package [24]).

The AMBER force field used in this study [25,26] does not contain force constants needed to describe modified parts of the 3cp5/3pc5 phosphonate analogs. The force field parameters were therefore completed with those obtained from ab initio calculations consistently with the original approach [25]. Force constants (see Table S1) were fitted to achieve the agreement of ~1 kcal/mol between QM (MP2/6-31G*) and MM relative energies of different conformers of the CH_3-O-PO_2-CH_2-O-CH_3 model system.

Almost half of the proteome of living organisms is constituted of metalloproteins. In the PDB database, magnesium ions are invariantly hexacoordinated with octahedral geometry. An analysis of structures available in the PDB to the 2002 indicated that the Mg—O bond length can range between 2.05 and 2.25 Å [21]. Unfortunately, the ability of the current generation of molecular dynamics pairwise-additive force fields to properly describe metal pockets is severely lacking due to the intrinsic difficulty of handling polarization and charge transfer contributions [27]. Magnesium ions are usually represented as van der Waals (VdW) spheres with a formal point charge +2 that interact with the protein environment and the substrate through non-bonded interactions. In binuclear active sites, however, high charges can lead to repulsion between two Mg^{2+} and instabilities, resulting in an alteration of the proper coordination of Mg^{2+} ions by ligands [21,28,29].

A consistent set of empirical interaction parameters for the alkali and alkaline-earth metal cations was derived by Aqvist using free energy perturbation simulations in aqueous solution [30]. When used these parameters for Mg^{2+} (as rescaled for AMBER: R^* = 0.7926 Å, epsilon = 0.8947), the coordination of both Mg(b) and Mg(c) in the β-polymerase active site changed [21]: Mg(b) lost contact with Asp192 and O2B (a non-bridging β-phosphate oxygen of the dNTP) and was instead coordinated by O3B (the oxygen bridging the β and γ phosphates of the dNTP); Mg(c) lost contact with the O3′ of the primer and O1A (a non-bridging α-phosphate oxygen of the dNTP coordinating both metal ions in the crystal structure).

Further, a general tendency to underestimate slightly magnesium-ligand distances, leading to a more compact active site, is usually observed in MD simulations [27,30]. The Aqvist parameters reproduce the observed hydration free energies as well as radial distribution functions of ions reasonably. However, the value of radius for Mg^{2+} ions (i.e. R^* = 0.7926 used in the AMBER force-filed) shows a less good agreement with the observed distance than for any of the other ions and appears to be slightly too small [30]. Even though using Mg^{2+} with R^* = 1.300 Å and epsilon 0.06 yielded the best structural results among the traditional one-atom Mg^{2+} models, there were some significant discrepancies between the crystal structures and the modeled structures, i.e. increased Mg(b)—Mg(c), O1A—Mg(b) distances [21].

The Aqvist–Warshel (AW) model that uses cationic dummy atoms and has proven very useful in accurately representing the energetics and structures of systems with transition metals such as octahedrally coordinated bivalent manganese ions and tetrahedrally coordinated bivalent zinc ions in mononuclear and binuclear metalloenzymes [21]. The AW model allows for stable coordination

geometry by placing the cationic dummy atoms at the defined positions around the central metal atom and for a smaller repulsion between the metal ions in binuclear sites by distributing the positive charge over the cationic dummy atoms. In [21], the AW model always performed better than the best traditional one-atom Mg^{2+} model. In particular, the Mg(b)—Mg(c) distance and the distance between Mg(b) and O1A of the incoming dNTP were much closer to the X-ray crystallographic distances. Further, in the case of the RNA ligase ribozyme [31], the Mg—O bond lengths obtained via a dummy approach [21] were more similar to those measured in QM/MM MD simulations and in the X-ray structures of other Mg^{2+} containing enzymes.

The AW model was used here for a preliminary MD simulation (lasting for 1000 ns) of HS RNase H enzyme in complex with unmodified nucleic acids. The active site of HS RNase H was stable (see Graph S14). Nevertheless, we would like to carry out comparative MD simulations of various RNase H/Argonaute enzymes with the use of multiple crystal structures for each of them. From this perspective, however, we felt the AW model a little bit complicated and uncomfortable for fast building of simulated systems. Especially when the enzyme active site is not our primary concern and we want just to ensure its stability during MD simulations.

Therefore, we decided to fine-tune an empirical one-atom model of Mg^{2+} so that the results of MD simulations were close to what was observed with the AW model in our preliminary MD simulation. We have taken into account that problems with binuclear active sites arise because of the neglect of polarization. One possibility would be to change the point charges on both ions and all of its ligands (which again is not practical if you want to work with many crystal structures). In [21], in the best one-atom Mg^{2+} model both the Mg(b)—Mg(c) distance and the Mg(b)—O1A distance deviated significantly from the crystal structure by up to 13% and 18%, respectively. It was recognized that these distances are likely correlated, because O1A as a bridging ligand keeps the Mg(b)—Mg(c) distance short. The point charges of the non-bridging pro-Sp (analogous to O1A in [21]) and pro-Rp oxygen of the scissile rA5-rC6 phosphate group which undergoes contacts with both magnesium ions in the HS RNase H active site were modified here (from −0.7761/−0.7761 to −0.9761/−0.5761). Further, a general tendency to underestimate slightly magnesium-ligand distances, leading to a more compact active site, which is usually observed in MD simulations [27,30], was considered. Therefore, the radius R^* of Mg^{2+} was changed from 0.7926 to 1.1 Å (recall that $R^* = 1.3$ Å was used in the best one-atom model in [21]).

Equilibration MD trajectories lasting for 5 ns were computed with the aid of the NAMD 2.7 software package [32]. The smooth Particle-mesh Ewald (PME) method was employed for long-range electrostatic forces [33]. The non-bonded cutoff was set to 9 Å. The SHAKE algorithm (tolerance 0.0005) was applied to constrain bonds where the hydrogen atoms were involved [34]. Simulated systems were energy minimized, then the Langevin dynamics was used for a temperature control [32]. The simulated systems were heated from 0 K to 310 K. The Langevin piston method was applied to reach an efficient pressure control with target pressure set to 1 atm [32]. The integration timestep was set to 2 fs. A multiprocessor system equipped with 16 Intel Itaninum CPUs (1.5 GHz) was used for equilibration MD simulations (computed at ∼4 ns/day for RNase H and <2 ns/day for TtAGO).

For production runs we have used ACEMD v. 2591 [35,36] running on a local workstation equipped with an NVIDIA graphics processing unit (GPU). ACEMD is a new generation molecular dynamics software which runs exclusively on GPUs at the equivalent speed of tens to hundred of standard processors. ACEMD implements all features of an MD simulation on a CUDA-compatible GPU device, including those usually required for production simulations in the NVT ensemble (i.e. bonded and nonbonded force term computation, velocity-Verlet integration, Langevin thermostatic control, smooth PME, and hydrogen bond constraints implemented using the M-shake algorithm and RATTLE for velocity constraints within the velocity Verlet integration scheme [37,38]). ACEMD does not presently contain a barostat for production runs, so simulations in the NPT ensemble are not possible. However, it is noted that with large molecular systems, changes in volume due to the pressure control are very limited after an initial equilibration making NVT simulations viable for production runs [35,36]. It was proven on multiple biomolecular systems including membrane proteins [39–41]. Therefore, our production runs have been performed in the NVT ensemble, Langevin thermostat at 310 K, computing the electrostatic interactions with PME. Also implemented in ACEMD is the hydrogen mass repartitioning scheme (the mass of the bonded heavy atoms to hydrogen is repartitioned among hydrogen atoms, leaving the total mass of the system unchanged) used, for instance, in codes such as Gromacs, which allows an increased time step of up to 4 fs [35,42]. Therefore, the integration timestep in our production MD runs was set to 4 fs. For production MD runs (1000 ns + 2 × 200 ns = 1400 ns for RNase H, 500 ns for TtAGO) CUDA programmable NVIDIA GTX-580 GPU equipped with 480 cores were used. MD trajectories were computed at ∼50 ns/day for RNase H and ∼20 ns/day for TtAGO (i.e. ∼53 days of GPU time in total).

Data were recorded every 100 ps. MD trajectories were analyzed with the aid of the CHIMERA 1.5.3, VMD 1.9, Curves+ and AMBER10/ptraj software packages [24,43–45]. Figures were produced by means of the ICM Molsoft 3.7 software package.

3. Results

3.1. HS RNase H – DNA recognition

Five internucleotide linkages (taken from the 3′ end of DNA) are involved in stabilizing interactions with the HS RNAse H surface (see Fig. 1). The first two internucleotide linkages (dG1-dC2-dT3) interact with the core of HS RNAse H that is formed by either hydrophobic (Ile, Val, Phe) or bulky (Trp) side chains. The third internucleotide linkage (dT3-dG4) binds to the so called phosphate binding pocket (see Fig. S1). The fourth (dG4-dT5) and fifth (dT5-dG6) internucleotide linkages could potentially interact with Arg153-5, Arg157 residues in the extremely basic loop of HS RNase H.

In the sugar-phosphate backbone of DNA, highly charged phosphate groups alternate with rather hydrophobic deoxyribose moieties. The DNA binding surface of HS RNase H mirrors nucleic acids. Polar regions alternate with hydrophobic clusters as well. In the HS RNase H + DNA:RNA complex, phosphate groups and amino acids side chains are bound by intermolecular hydrogen bonds (Trp, Asn, Thr) or salt bridges (Lys, Arg). In addition, clusters of hydrophobic (Ile, Val, Phe) or partly hydrophobic (Thr) amino acids side chains establish favorable VdW contacts with rather hydrophobic deoxyribose moieties of DNA.

3.2. 1st DNA-binding site – 3pc5 MD (Fig. 2, Graph 1A: Trp225 red line, Ser233 blue line)

The first DNA-binding site is a channel formed by Trp221, Trp225, and Ser233 in the basic protrusion of HS RNase H [20] (homologous residues in EC RNase H are Trp81 and Trp85 [19]; BH RNase H lacks the basic protrusion completely [46]).

In our MD simulations, the 3pc5 phosphonate group of the first dG1-dC2 internucleotide linkage was hydrogen bonded toward Trp225 and Ser233. The interaction with Trp225 was remarkably

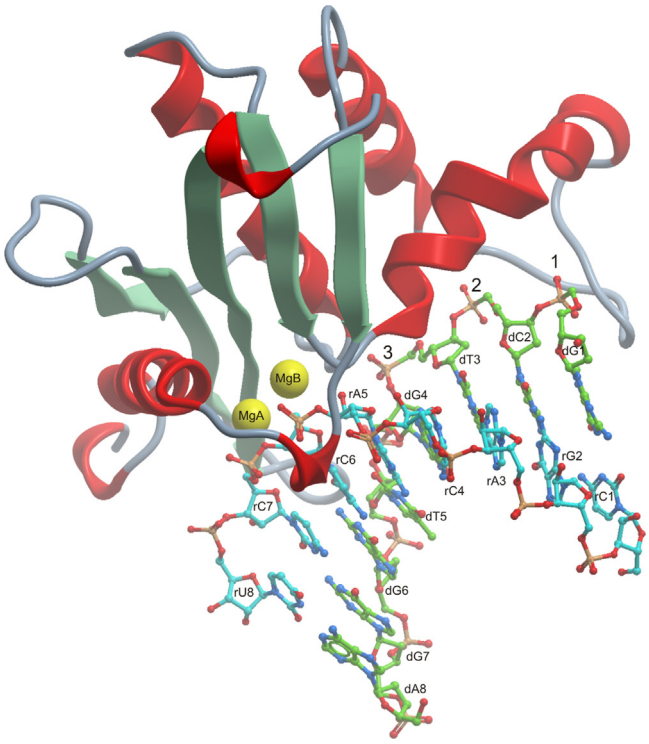

Fig. 1. Five internucleotide linkages from the 3′ end of DNA are involved in stabilizing interactions with the HS RNAse H surface.

stable despite of conformational promiscuity of the dG1-dC2 internucleotide linkage and instabilities found in the rC1.dG1 Watson–Crick base pair (see below). In contrast, there were several short living interruptions in mutual contacts of dG1-dC2 with Ser233.

The dG1 and dC2 deoxyribose moieties as well as the -CH_2- group wedged in the dG1-dC2 phosphonate internucleotide linkage were in close contacts with the Trp221 side chain, which probably helps to distinguish DNA:RNA and RNA:RNA hybrids (the 2′-OH group of RNA modeled into the DNA binding channel of HS RNase H clashes with the indole ring of Trp221 [20]).

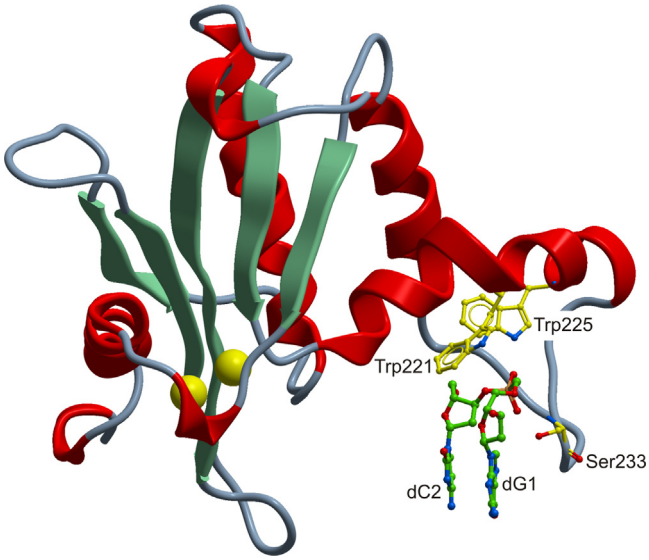

Fig. 2. The 3pc5 dG1-dG2 internucleotide linkage binding into the 1st DNA binding site.

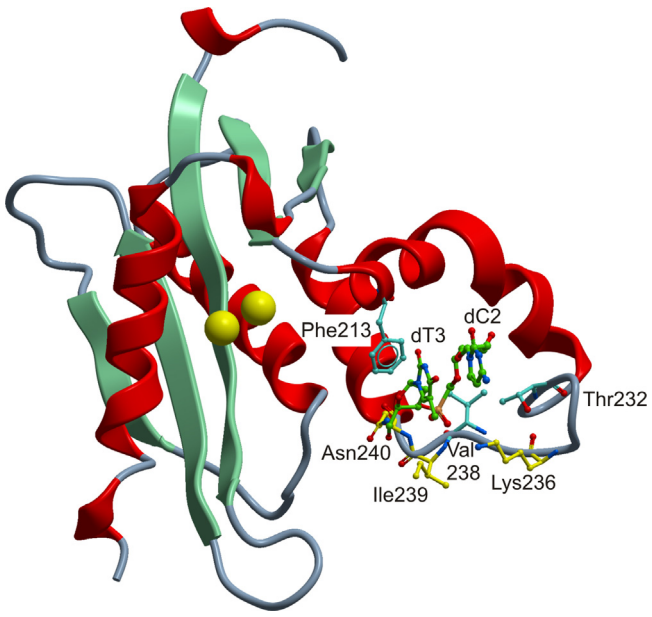

Fig. 3. The 3pc5 dC2-dT3 internucleotide linkage binding into the 2nd DNA binding site.

3.3. 2nd DNA-binding site – 3pc5 MD (Fig. 3, Graph 1B: Asn240 m.c. blue line, Ile239 m.c. cyan line, Asn240 s.c. red, Lys236 s.c. green line)

The second DNA-binding site, where the 3pc5 phoshonate group of dC2-dT3 was anchored, consisted of main chain amide groups of Asn240 and Ile239, which were occasionally accompanied by side chains of Asn240 and Lys236.

Further, there were observed VdW contacts between the bulky side chain of Phe213 and the dT3 deoxyribose moiety and between the Thr232, Val238 side chains and the —CH_2— group of the dC2-dT3 phosphonate internucleotide linkage.

In [20], the second DNA-binding site was not explicitly mentioned as the natural phosphate internucleotide linkage was buried substantially less deeply into the HS RNase H surface. In the case of EC RNase H, the phosphate/phosphonate groups were potently stabilized by polar interactions with side chains of Tyr73, Trp104 and Lys99 [19] (replacing Phe213, Phe244, Ile239 of HS RNase H).

3.4. 3rd DNA binding site – 3pc5 MD (Fig. 4, Graph 1C1: Thr181 blue line, Asn240 red line; Graph1C2: Gln183 blue line, Asn182 green line, Arg184 cyan line, Asn240 red line)

The 3pc5 phosphonate group of the dT3-dG4 internucleotide linkage established contacts with the main chain amide group of Gln183. Moreover, the Asn240 side chain was loosely bound to the atom O5′ of the 3pc5 phosphonate group.

In [20], the dT3-dG4 phosphate group was bound to Thr181, Arg179 and Asn240. A similar phosphate-binding pocket was found in BH RNase H [46]. The pockets are spatially conserved but share only one conserved residue, Thr181 in HS RNase H and Thr104 in BH RNase H. Interestingly, analogous Thr43 in EC RNase H was identified as interacting with DNA by one of us before [19].

Sensitivity of the phosphate binding pocket to modified internucleotide linkages was evidenced by experimental results [47]. This can be explained on the basis of structural information. In HS RNase H, Both Thr181 (in the phosphate binding pocket) and Glu186 (in the active site) are located on the same α-helix (Fig. S1). Therefore, any suboptimal binding of modified internucleotide linkages into the phosphate binding pocket can lead to an allosteric modulation of the HS RNase H active site.

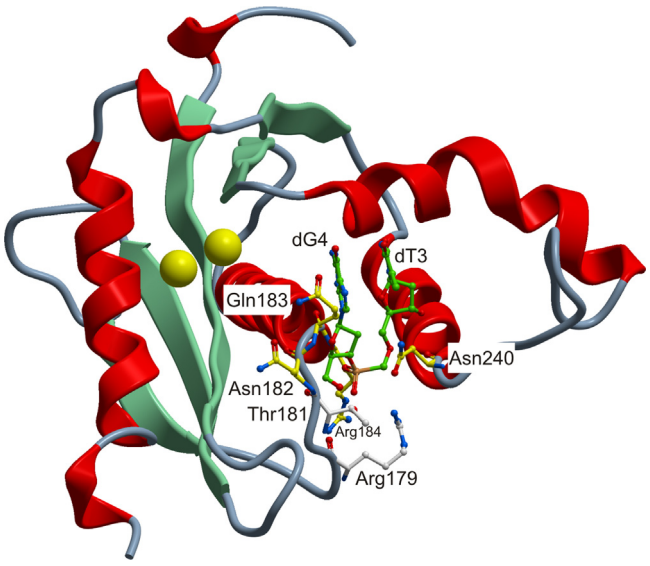

Fig. 4. The 3pc5 dT3-dG4 internucleotide linkage binding into the 3rd DNA binding site.

Crystal structures show that to place just a natural dT3-dG4 internucleotide linkage into the phosphate binding pocket requires large distortions of the backbone torsion angles (γ and α) by ∼150° from the ideal values [20]. Indeed, in our preparatory MD simulations with natural oligonucleotides, the Thr181 – dT3-dG4 contacts were lost when the lowest energy conformer **-g-g** (in terms of the C3′-O3′-P-O5′, O3′-P-O5′-C5′ torsion angles) was realized. It imposes increased demands on potential antisense oligonucleotides, as modified internucleotide linkages must be able to mimic the phosphate group adopting not only its natural lowest-energy conformer **-g-g**. This hurdle can be by-passed by oligonucleotide gapmers or oligonucleotides with alternating natural and modified internucleotide linkages.

It seems to be the case of the 3pc5 phosphonates, which elicit the RNase H activity only if they alternate in oligonucleotide with natural internucleotide linkages [15]. In our MD simulations, the 3pc5 phosphonate group of the dT3-dG4 internucleotide linkage lacked contacts with Thr181 in the phosphate binding pocket. Therefore, it seems likely that oligonucleotides with alternating phosphate/3pc5-phosphonate internucleotide linkages will be rather active when the 3pc5 phosphonate will bind to the second DNA binding site and the first and third (phosphate binding pocket) DNA binding site will be occupied by natural internucleotide linkages.

3.5. 4–5th DNA binding site – 3pc5 MD (Fig. S2, Graph 1D: Asn151 red line, Arg153 blue line)

The phosphate group of the natural dG4-dT5 internucleotide linkage was in contact with Asn151. The natural dT5-dG6 internucleotide linkage interacted with Arg153. These contacts were established after elapsing of about 30 ns. Arg153 altogether with Arg154, Arg155 and Arg157 forms the basic loop in HS RNase H structures, where significant differences among HS RNase H crystal structures were observed [20]. Our preliminary MD simulations with natural substrates showed that neither the trajectories lasting for 1 us are sufficient for a complete conformational relaxation of this basic loop. Therefore, it cannot be excluded that the dG4-dT5 and dT5-dG6 internucleotide linkage come to contact with Arg154, Arg155 and Arg157 on longer time scales. Anyway, the Arg residues would be probably involved in the initial enzyme-substrate recognition (as proposed in [20]).

3.6. 1st – 5th DNA binding site – 3cp5 MD (Graph 2A–D)

In contrast to what was observed for 3pc5 phosphonates, the 3cp5 phosponate internucleotide linkages lost contacts with HS RNase H DNA binding sites within several tens of ns. It's in agreement with known experimental data as the 3cp5 phosphonate oligonucleotides are not able to elicit the RNase H activity [15].

3.7. RNA–HS RNase H interactions – (Fig. S3, Graph S1: Glu186 blue and salmon line, Met212 red line, Arg278 green line)

The HS RNase H active site is located in the RNA-binding groove, which interacts with the 2′-OH groups of four consecutive ribonucleotides (rC4, rA5, rC6, rC7 – two on each side of the scissile phosphate). The overall mechanism for RNA strand recognition is conserved [20] (as RNA strands complexed with HS, EC and BH RNase H superimpose well).

In our MD simulations, the RNA–HS RNase H contacts were mediated mostly by the side chain of Glu186 interacting with the 2′-OH group of rA5. Recall that Glu186 is bound to Mg^{2+} in the HS RNase H active site. Further, as we speculate above, Glu186 could transmit allosteric signals from the phosphate binding pocket to active site of HS RNase H.

The main chain atoms of Met212 were involved in contacts with rC4 – especially in the second half of the 3pc5 MD simulation.

Contacts of the Cys148, Ser150 and Asn151 backbone atoms with the rC6 and rC7 2′-OH groups were rather poor, however, it could be partly rooted in the insufficient relaxation of the 153–157 basic loop, where significant differences among individual HS RNase H structures were observed [20].

Interactions between RNA and Arg residues were very sporadic. The only exception was the rC6-rC7 internucleotide linkage and Arg278. rC6-rC7 is located just behind the scissile rA5-rC6. Therefore, the Arg278–rC6-rC7 contacts could help to stabilize the reaction product. Moreover, the rC6-rC7 internucleotide linkage could trap the proton released from the catalytic water molecule. It could facilitate formation of the hydroxide ion that attacks the scissile rA5-rC6 internucleotide linkage. The Arg278 side chain was situated differently in the 3pc5/3cp5 MD simulations. Therefore, remarkable differences were observed in terms of contacts of the catalytic water molecule with both the rC6-rC7 as well as rA5-rC6 internucleotide linkages (see below).

3.8. Helical parameters (Graph S2-S5)

Helical parameters of both 3pc5/3cp5-DNA:RNA duplexes were calculated by means of the Curves+ program [45]. The most affected helical parameters were Buckle, Shift, Slide and Rise. As a result of the distorted DNA strand, the minor groove width of the DNA:RNA duplex varies form 7.36 Å (3pc5)//7.76 Å (3cp5) at the phosphate-binding pocket to 10.92/11.34 Å (3pc5)//11.14/11.48 (3cp5) at terminal parts of the DNA/RNA hybrid.

It means, that both 3pc5/3cp5-DNA:RNA duplexes were remarkably distorted despite of the 3cp5 DNA strand dissociation from the HS RNase H surface. Neither the 200 ns MD simulation was sufficient to achieve a full relaxation of the 3cp5-DNA:RNA duplex geometry. Apparently, deformations are dictated by the overall shape of HS RNase H rather than by detail interactions of phosphate/phosphonate groups with specific amino acids in DNA binding sites. In accordance with that no such variations were observed in complexes of BH RNase H, which lacks the basic protrusion [46] (Fig. S1).

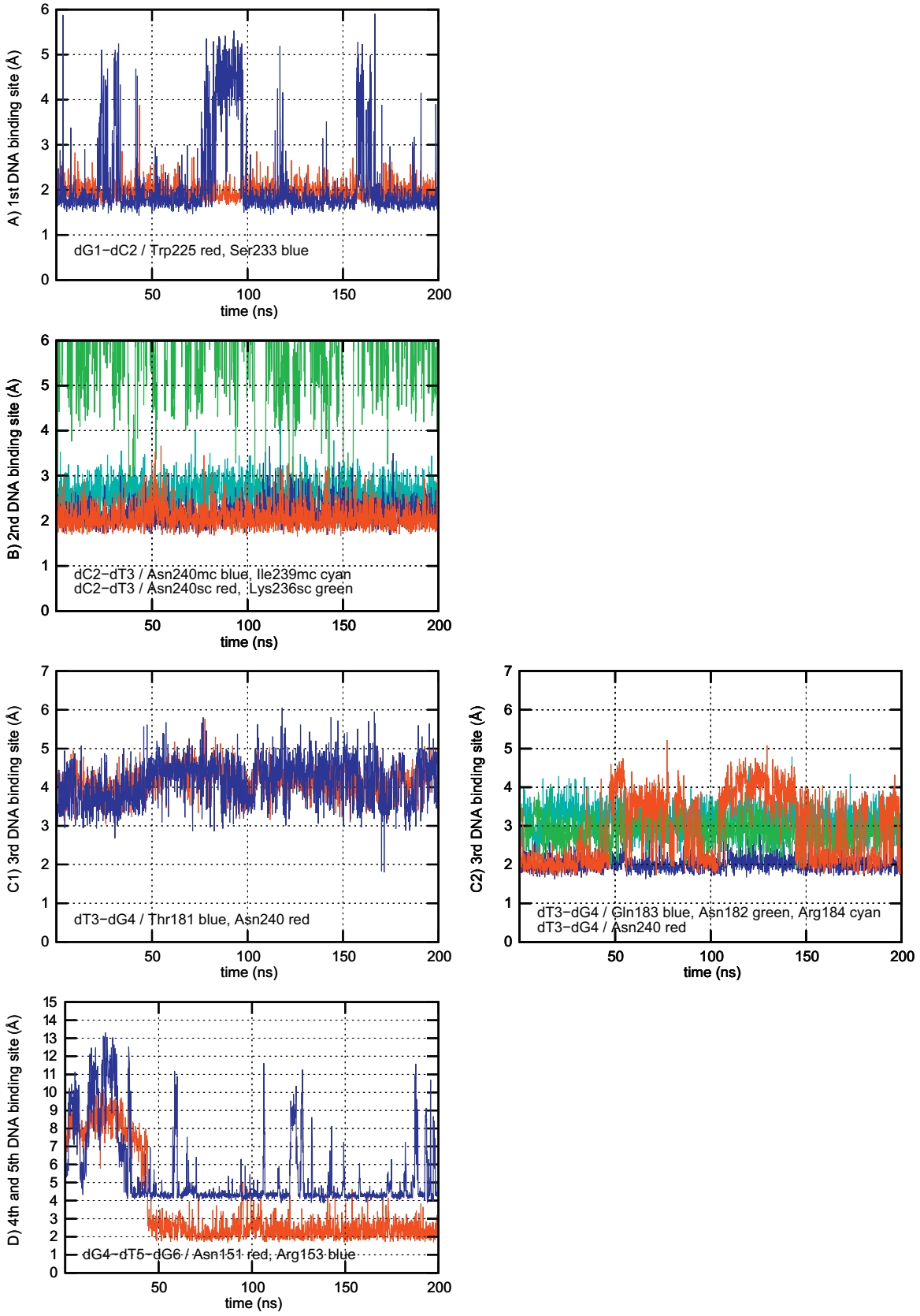

Graph 1. 3pc5 DNA recognition by DNA binding sites of HS RNase H: (A) Trp225 – red line, Ser233 – blue line; (B) Asn240 m.c. – blue line, Ile239 m.c. – cyan line, Asn240 s.c. – red line, Lys236 s.c. – green line; (C1) Thr181 – blue line, Asn240 – red line; (C2) Gln183 – blue line, Asn182 – green line, Arg184 – cyan line, Asn240 – red line; (D) Asn151 – red line, Arg153 – blue line (For interpretation of the references to color in this figure legend, the reader is referred to the web version of the article.).

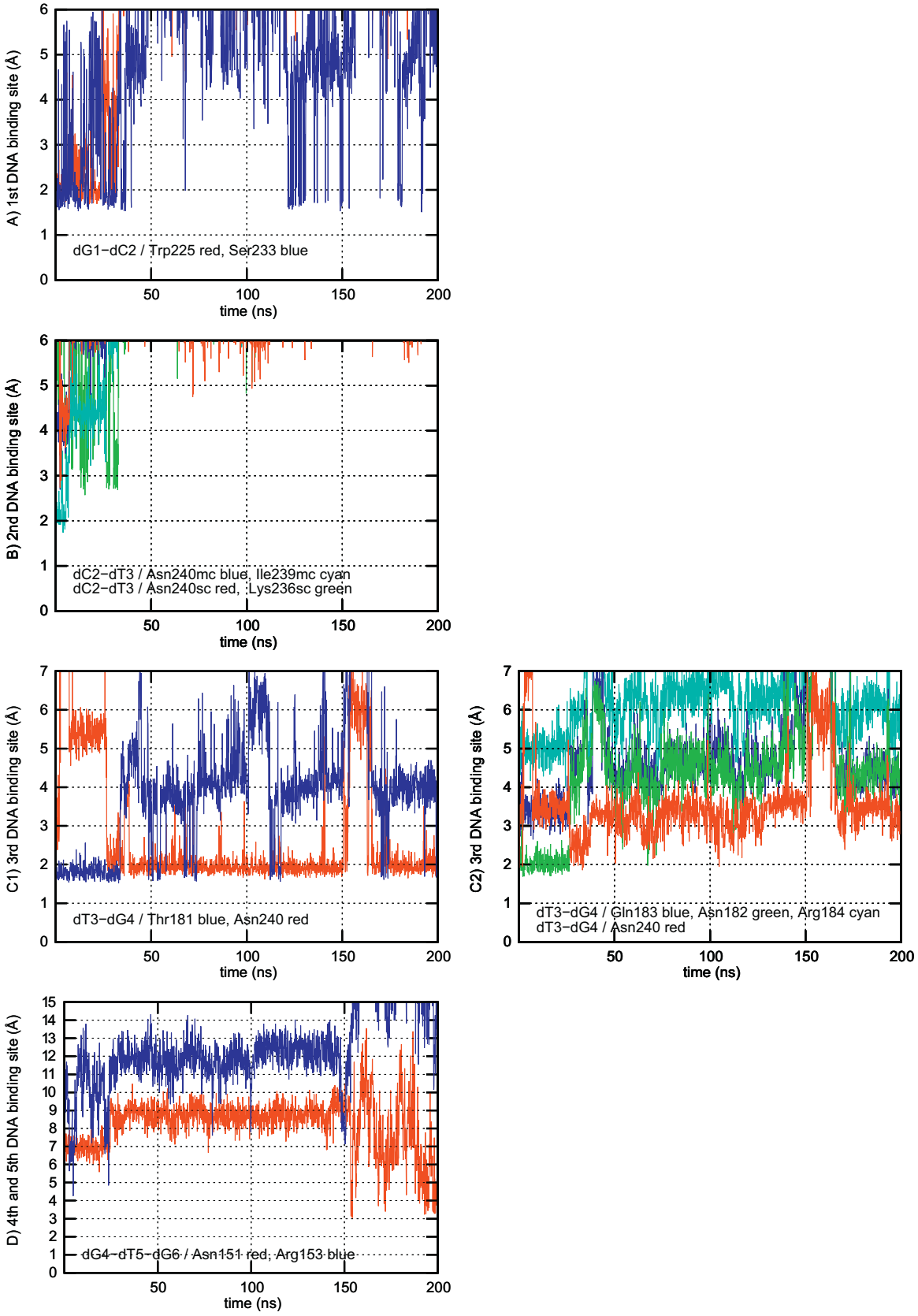

Graph 2. 3cp5 DNA recognition by DNA binding sites of HS RNase H: (A) Trp225 – red line, Ser233 – blue line; (B) Asn240 – blue line, Ile239 – cyan line, Asn240 – red line, Lys236 – green line; (C1) Thr181 – blue line, Asn240 – red line; (C2) Gln183 – blue line, Asn182 – green line, Arg184 – cyan line, Asn240 – red line; (D) Asn151 – red line, Arg153 – blue line (For interpretation of the references to color in this figure legend, the reader is referred to the web version of the article.).

3.9. Watson–Crick hydrogen bonding (Graph S6)

In both MD simulations, the Watson–Crick hydrogen bonds were stable with the exception of terminal base pairs. Nevertheless, such occasional fraying of nucleic acids ends is commonly observed in MD simulations even in the case of double helical structures, which are unaffected by interactions with enzymes.

3.10. Sugar puckering (Graph S7–S10)

The RNA strand was in the regular A-form with sugars in **C3′-endo**. Nevertheless, **C2′-exo** was remarkably populated in the phosphate binding pocket and **C4′-exo** in terminal parts of both 3pc5/3cp5-DNA:RNA structures.

The 3pc5 DNA strand was mostly in the B-form (with sugars between **C2′-endo** and **O4′-endo**) except for dC2 and dT3 in the DNA-binding channel, which were in **C4′-exo** (i.e. between the A and B form). In the 3cp5 DNA only dT3 was in **C4′-exo**. It indicates a partial relaxation of 3cp5 DNA after its dissociation from the HS RNase H surface.

3.11. Phosphonate internucleotide linkages (Graph S11)

All 3pc5/3cp5 phosphonate internucleotide linkages were conformationally promiscuous (in terms of either the C3′-O3′-**P-C**, O3′-**P-C**-O5′, **P-C**-O5′-C5′ or C3′-O3′-**C-P**, O3′-**C-P**-O5′, **C-P**-O5′-C5′ torsion angles). This is evident especially in the case of the 3cp5 internucleotide linkages, which lost contacts with the DNA binding sites on the HS RNase H surface. However, even the 3pc5 internucleotide linkages that were steadily bound to all DNA binding sites fluctuated between several conformational basins.

3.12. Phosphate internucleotide linkages (Graph S7–S10)

Phosphate internucleotide linkages in DNA (i.e. dG4-dT5-dG6-dG7-dA8) adopted the lowest energy conformer **-g-g** (i.e. **-gauche** in terms of the C3′-O3′-P-O5′, O3′-P-O5′-C5′ torsion angles). Phosphate internucleotide linkages in RNA preferred **-g-g** as well.

Higher populations of **t-g** in rA3-rC4 indicate a suboptimal binding of DNA:RNA to the HS RNase H surface at the beginning of the 3cp5 MD simulation.

In X-ray structures [20], the rC4-rA5 internucleotide linkage was distorted from **-g-g**, which was preferred in both MD simulations. Similarly, the rC6-rC7 internucleotide linkage adopted an atypical conformation (or maybe an averaged mixture of conformers was observed) in crystals [20]. In MD simulations, the rC6-rC7 phosphate preferred the lowest energy conformer **-g-g** with occasional oscillations to **t-g**. Recall that rC6-rC7 was in contact with Arg274.

3.13. Active site – MgA and MgB (Fig. 5, 3pc5 Graph S12A, 3cp5 Graph S13A, 7p AW model Graph S14A, TtAGO Graph S15A)

The HS RNase H active site is superimposable with that of either BH RNase H or EC RNase H, including the scissile phosphate. Two Mg^{2+} ions occupy the canonical A and B positions. It's assumed that the two-metal ion mechanism for catalysis is universally shared [48]. Both 3pc5/3cp5 MD simulations produced trajectories that were stable consider the distance separating both magnesium ions. That is not entirely obvious in binuclear active sites [21] (see Section 4).

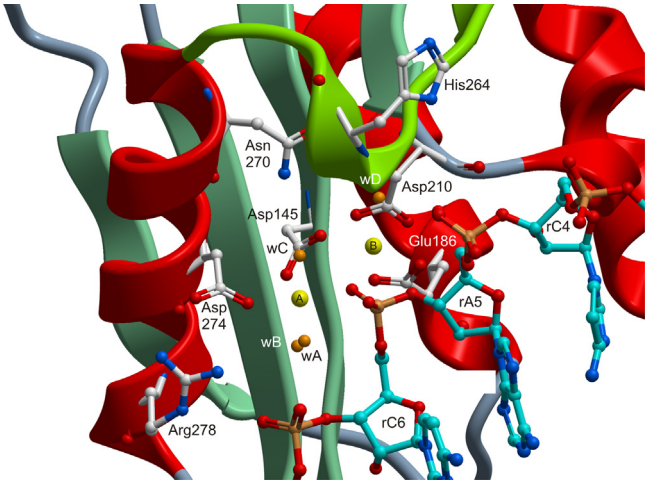

Fig. 5. HS RNase H active site.

3.14. MgA coordination shell – 3pc5 MD (Fig. 5, Graph S12C1: Asp274 red line, Asp145 green line, Sp blue line; Graph S12C2: WATA-C; Graph S12B: WATA)

Magnesium ion A was coordinated in the octahedral configuration by Asp145, Asp274, the pro-Sp non-bridging oxygen atom of the scissile rA5-rC6 phosphate and three water molecules. The water molecule that attacks the scissile rA5-rC6 phosphate will be referred as WATA in the following text.

Throughout the whole 3pc5 MD run, the oxygen atom of WATA protruded into the immediate vicinity (below the 3 Å treshold) of the phosphorus atom of the scissile rA5-rC6 internucleotide linkage. Hydrogen atoms of WATA made contacts with the adjacent rC6-rC7 internucleotide linkage. Both events may be favorable for the reaction.

3.15. MgA coordination shell – 3cp5 MD (Fig. 5, Graph S13C1: Asp274 red line, Asp145 green line, Sp blue line; Graph S13C2: WATA-C; Graph S13B: WATA)

Water molecules interchanged repeatedly in the WATA position within the 3cp5 MD run. The oxygen atom of WATA protruded less frequently below the 3 Å threshold consider the distance from the phosphorus atom of the scissile rA5-rC6 internucleotide linkage. Hydrogen atoms of WATA made contacts with the adjacent rC6-rC7 internucleotide linkage only occasionally.

This was mainly due to different (comparing to 3pc5 MD) conformational preferences of the Arg278 side chain interacting with the rC6-rC7 internucleotide linkage.

3.16. MgB coordination shell-

3pc5 MD (Graph S12D1: Asp145 red line, Glu186 green line, Glu186 blue line, Asp210 cyan line, Asp210 magenta line, Sp yellow line, O3′ salmon line, Graph S12D2: WAT).

3cp5 MD (Graph S13D1: Asp145 red line, Glu186 green line, Glu186 blue line, Asp210 cyan line, Asp210 magenta line, Sp yellow line, O3′ salmon line, Graph S13D2: WAT).

In X-ray structures [20], MgB is coordinated by five ligands: Asp145, Glu186, Asp210 (or Asn210), the O3′ and pro-Sp non-bridging oxygen atoms of the scissile rA5-rC6 phosphate group. In our MD simulations, subtle differences were observed consider the 3rd-6th ligands:

1st ligand: The non-bridge pro-Sp oxygen atom of the rA5-rC6 scissile internucleotide linkage was tied quite symmetrically between MgA and MgB.

2nd ligand: Similarly, the side chain of Asp145 was bound simultaneously to MgA and MgB.
3rd ligand: The side chain of Asp210 had a tendency to provide both oxygen atoms toward MgB and thus create a so-called bi-dentate contact.
4th ligand: Similarly, Glu186 tend to form bi-dentate contacts with MgB.
5th ligand: The O3′ atom of the rA5-rC6 scissile internucleotide linkage was weakly bound to MgB in the first half of the 3pc5 MD run. Then even more loosened contacts prevailed. In the 3cp5 MD simulation, this process was faster and even more pronounced.
6th ligand: Several water molecules reside close to MgB in the RNase H interior (see WD in Fig. 5). Roughly in the half of both MD simulations water molecules expelled the O3′ atom of the rA5-rC6 scissile internucleotide linkage from MgB. It was more pronounced in the 3cp5 MD simulation, in fact, there were many molecules interchanging in this position in the 3pc5 MD simulation.

Altogether, Asp210 and Glu186 tendency to form bi-dentate contacts with MgB led to rather over-coordinated (7 ligands) MgB. This tendency was even more pronounced in reference MD simulations with the seven-point representation of magnesium ions (compare Graph S12 and Graph S14).

In the TtAGO MD simulation (Fig. S1, Graph S15), Asp546 (Asp210 in HS RNase H) was mono-dentate and Glu512 (Glu186 in HS RNase H) bi-dentate.

4. Discussion and conclusions

Our 200 ns MD simulations show that fully modified oligonucleotides bearing the 3′-O-P-CH_2-O-5′ (but not 3′-O-CH_2-P-O-5′) phosphonate linkages can be attached to the HS RNase H surface (compare Graph 1 with Graph 2). It enables to explain that oligonucleotides consisting of the alternating 3′-O-P-CH_2-O-5′-phosphonate and phosphodiester linkages are capable to elicit the RNase H activity (while the 3′-O-CH_2-P-O-5′-phosphonates are completely inactive) [15].

In binuclear active sites, which are modeled using non-polarizable force fields, the artificial repulsion arising between both magnesium ions can lead to severe instabilities and alterations of the proper coordination of magnesium ions by ligands [21]. Therefore, the polarized rA5-rC6 scissile phosphate (with the non-bridging oxygen atom wedged between magnesium ions) was used in our MD simulations. Further, a general tendency to underestimate slightly magnesium-ligand distances, leading to a more compact active site, is usually observed in MD simulations [27,30]. Therefore, the radius R^* of Mg^{2+} was changed from 0.7926 to 1.1 Å (recall that even greater value of 1.3 Å was used in the best one-atom model of Mg^{2+} in [21]). The resulting MgA-MgB distances found in our MD simulations were stable on the time scale of hundreds of nanoseconds (Graph S12–13). A reference MD simulation (lasting for 1000 ns) produced using the seven-point (with dummy atoms) AW representation of magnesium ions [21] led to almost the same results (compare Graph S12 and Graph S14). Therefore, the usage of a partial polarization of the scissile internucleotide linkage (which is easier for implementation than the AW model [21]) is justified especially in studies, where the enzyme active site is not a primary concern. Further, fluctuations around average values were a little bit more pronounced in our model (Graph S12) comparing to the AW model [21] (Graph S14). In fact, larger radius of Mg^{2+} led to a modest diminishing of stabilizing coulombic interactions acting between ions and ligands. Therefore, active sites in our MD simulations were inevitably a little bit understabilized. In subsequent studies, we want to destabilize ion-ligand interactions even much more to enable a proper relaxation (at an acceptable time scale) of loops around the RNase H/Argonaute active site, which could be the subject of crystal packing forces or artifacts due to point mutations applied in X-ray structures.

Further, to demonstrate its transferability, we applied our approach chosen for the stabilization of binuclear active sites to TtAGO [22], where the metal-binding residue Glu512 (analogous to Glu186 in HS RNase H) is in a very labile position. In fact, only quite recently was recognized that Argonaute enzymes use the catalytic tetrad rather than catalytic triad of residues [14] (Fig. S1). The Argonaute active site was completely stable in the MD run lasting for 500 ns (Graph S15). As proposed in [14], Glu512 was bound in the TtAGO active site in exactly the same way as Glu186 was bound in the HS RNase H active site (i.e. Glu186/512 interacted with both the 2′-OH of the nucleotide adjacent to the scissile phosphate and one of the two active-site divalent metal ions, Fig. 5).

Glu186 in the HS RNase H active site is close to conserved Thr181 in the so called phosphate-binding pocket (Fig. S1) sensitive to chemical modifications of antisense oligonucleotides [47]. We speculate that an allosteric signal could be transmitted from Thr181 to Glu186 in the case of a suboptimal binding of modified internucleotide linkages (including here presented 3pc5 phosphonates – Graph 1C1) into the phosphate-binding pocket.

In the case of TtAGO, main chain atoms of Glu512 interact directly with the phosphate group of siRNA at position 13–14 (Fig. S1). Therefore, chemical modifications of siRNA backbones can act on the TtAGO active site quite straightforwardly. Indeed, significantly lower AGO2 cleavage activities were observed for the antisense RNAs containing a 2′-MOE substitution at positions 2, 13, and 14 [49,50]. Comparable binding affinities were observed for the antisense RNA containing the 2′-MOE substitutions at positions 12–14 compared with the unmodified antisense RNA. Taken together, these data suggest that the loss in AGO2 cleavage activity was due to the 2′-MOE residues interfering with catalysis [49,50].

In order to investigate an allosteric modulation of the RNase H/AGO active sites by Glu fingers precisely, it will need to address further, what exactly is the coordination of MgB in the moment immediately preceding the reaction event. It was speculated in [48] (based on crystal structures of BH RNase H) that under-coordinated MgB provides a driving force for the reaction. However, crystal structures are subjected to crystal packing forces, point mutations are carried out in their active sites (in order to prevent the reaction), different (Mg^{2+}/Ca^{2+}) ions are used for crystallization etc. Then, such as different form of bi-dentate/mono-dentate binding to MgB as observed here for analogous Asp210/Asp546 residues in HS RNase H/TtAgo can be found. In fact, Glu186 and Asp210 tendency to form bi-dentate contacts led to rather over-coordinated MgB in HS RNase H. It was even more pronounced with the AW model [21] applied in the reference MD simulation (compare Graph S12D1 with S14D1).

The balance between point charges on oxygen atoms of bio- and water molecules appears to be another moot point. Charges in TIP3P water molecules [23] were determined based on a completely different philosophy than RESP charges of biomolecules in the AMBER force field [25]. Therefore, probably, the O3′ atom of the scissile rA5-rC6 internucleotide linkage was expelled from MgB by water molecules residing in the HS RNase H interior. Interestingly, this artifact was again more pronounced in the reference MD simulation with the seven-point AW model for Mg^{2+} [21] (compare Graph S12D1 with S14D1).

Acknowledgments

This work was supported by the Grant Agency of the Czech Republic (202/09/0193). The access to computing and storage facilities owned by parties and projects contributing to the National Grid Infrastructure MetaCentrum, provided under the program “Projects

of Large Infrastructure for Research, Development, and Innovations" (LM2010005) is highly acknowledged.

Appendix A. Supplementary data

Supplementary data associated with this article can be found, in the online version, at http://dx.doi.org/10.1016/j.jmgm.2013.05.004.

References

[1] M.L. Jain, P.Y. Bruice, I.E. Szabo, T.C. Bruice, Incorporation of positively charged linkages into DNA and RNA backbones: a novel strategy for antigene and antisense agents, Chemical Reviews 112 (2012) 1284–1309.
[2] J. Kurreck, Antisense technologies. Improvement through novel chemical modifications, European Journal of Biochemistry 270 (2003) 1628–1644.
[3] Y.S. Cho-Chung, Antisense DNAs as targeted genetic medicine to treat cancer, Archives of Pharmacal Research 26 (2003) 183–191.
[4] J.B. Opalinska, A.M. Gewirtz, Nucleic-acid therapeutics: basic principles and recent applications, Nature Reviews Drug Discovery 1 (2002) 503–514.
[5] A. Dove, Antisense and sensibility, Nature Biotechnology 20 (2002) 121–124.
[6] D.B. Braasch, D.R. Corey, Novel antisense and peptide nucleic acid strategies for controlling gene expression, Biochemistry 41 (2002) 4503–4510.
[7] A.M. Gewirtz, D.L. Sokol, M.Z. Ratajczak, Nucleic acid therapeutics: state of the art and future prospects, Blood 92 (1998) 712–736.
[8] E. Uhlmann, A. Peyman, Antisense oligonucleotides a new therapeutic principle, Chemical Reviews 90 (1990) 544–584.
[9] S.T. Crooke, Vitravene – another piece in the mosaic, Antisense and Nucleic Acid Drug Development 8 (1998) vii–viii.
[10] S.T. Crooke, An overview of progress in antisense therapeutics, Antisense and Nucleic Acid Drug Development 8 (1998) 115–122.
[11] A. Fire, S.Q. Xu, M.K. Montgomery, S.A. Kostas, S.E. Driver, C.C. Mello, Potent and specific genetic interference by double-stranded RNA in Caenorhabditis elegans, Nature 391 (1998) 806–811.
[12] A.Z. Fire, Gene silencing by double-stranded RNA (Nobel Lecture), Angewandte Chemie International Edition 46 (2007) 6966–6984.
[13] Craig C. Mello, Return to the RNAi world: rethinking gene expression and evolution (Nobel Lecture), Angewandte Chemie International Edition 46 (2007) 6985–6994.
[14] K. Nakanishi, D.E. Weinberg, D.P. Bartel, D.J. Patel, Structure of yeast Argonaute with guide RNA, Nature 486 (2012) 368–374.
[15] D. Rejman, J. Snášel, R. Liboska, Z. Točík, O. Pačes, S. Králíková, M. Rinnová, P. Kois, I. Rosenberg, Oligonucleotides with isopolar phosphonate internucleotide linkage: a new perspective for antisense compounds? Nucleosides, Nucleotides and Nucleic Acids 20 (2001) 819–823.
[16] I. Barvík Jr., J. Štěpánek, J. Bok, Explicit solvent molecular dynamics simulation of duplex formed by the modified oligonucleotide with alternating phosphate/phosphonate internucleoside linkages and its natural counterpart, Journal of Biomolecular Structure and Dynamics 19 (2002) 863–875.
[17] J. Hanuš, I. Barvík Jr., J. Štepánek, P.-Y. Turpin, J. Bok, I. Rosenberg, M. Petrová, —CH_2— lengthening of the internucleotide linkage in the ApA dimer can improve its conformational compatibility with its natural polynucleotide counterpart, Nucleic Acids Research 29 (2001) 5182–5194.
[18] O. Páv, I. Košiová, I. Barvík, R. Pohl, M. Budyšínský, I. Rosenberg, Synthesis of oligoribonucleotides with phosphonate-modified linkages, Organic and Biomolecular Chemistry 9 (2011) 6120–6126.
[19] I. Barvík, *E. coli* RNase HI and the phosphonate-DNA/RNA hybrid: molecular dynamics simulations, Nucleosides, Nucleotides and Nucleic Acids 24 (2005) 435–441.
[20] M. Nowotny, S.A. Galdamakov, R. Ghirlando, S.M. Cerritelli, R.J. Crouch, W. Yang, Structure of human RNase H1 complexed with an RNA/DNA hybrid: insight into HIV reverse transcription, Molecular Cell 28 (2007) 264–276.
[21] P. Oelschlaegner, M. Klahn, W.A. Beard, S.H. Wilson, A. Warshel, Magnesium-cationic dummy atom molecules enhance representation of DNA polymerase beta in molecular dynamics simulations: improved accuracy in studies of structural features and mutational effects, Journal of Molecular Biology 366 (2007) 687–701.
[22] Y. Wang, S. Juranek, H. Li, G. Sheng, G.S. Wardle, T. Tuschl, D.J. Patel, Nucleation, propagation and cleavage of target RNAs in Ago silencing complexes, Nature 461 (2009) 754–762.
[23] W.L. Jorgensen, J. Chandrasekhar, J. Madura, M.L. Klein, Comparison of simple potential functions for simulating liquid water, Journal of Chemical Physics 79 (1983) 926–935.
[24] D.A. Pearlman, D.A. Case, J.W. Caldwell, W.R. Ross, T.E. Cheatham, S. DeBolt, D. Ferguson, G. Seibel, P. Kollman, AMBER, a package of computer programs for applying molecular mechanics normal mode analysis, molecular dynamics and free energy calculations to simulate the structural and energetic properties of molecules, Computer Physics Communications 91 (1995) 1–41.
[25] W.D. Cornell, P. Cieplak, C.I. Bayly, I.R. Gould, K.M. Merz, D.M. Ferguson, D.C. Spellmeyer, T. Fox, J.W. Caldwell, P.A. Kollman, A 2nd generation force-field for the simulation of proteins, nucleic-acids, and organic-molecules, Journal of the American Chemical Society 117 (1995) 5179–5197.
[26] A. Perez, I. Marchan, D. Svozil, J. Sponer, T.E. Cheatham III, Ch A. Laughton, M. Orozco, Refinement of the AMBER force field for nucleic acids: improving the description of alpha/gamma conformers, Biophysical Journal 92 (2007) 3817–3829.
[27] M. Dal Peraro, K. Spiegel, G. Lamoureux, M. De Vivo, W.F. De Grado, M.L. Klein, Modeling the charge distribution at metal sites in proteins for molecular dynamics simulations, Journal of Structural Biology 157 (2007) 444–453.
[28] Y. Xiang, P. Oelschlaeger, J. Florian, M.F. Goodman, A. Warshel, Simulating the effect of DNA polymerase mutations on transition-state energetics and fidelity: evaluating amino acid group contribution and allosteric coupling for ionized residues in Human Pol Beta, Biochemistry 45 (2006) 7036–7048.
[29] J. Florian, M.F. Goodman, A. Warshel, Computer simulation of the chemical catalysis of DNA polymerases: discriminating between alternative nucleotide insertion mechanisms for T7 DNA polymerase, Journal of the American Chemical Society 125 (2003) 8163–8177.
[30] J. Aqvist, Ion–water interaction potentials derived from free energy perturbation simulations, Journal of Physical Chemistry 94 (1990) 8021–8024.
[31] J. Sgrignani, A. Magistrato, The structural role of Mg^{2+} ions in a class I RNA polymerase ribozyme: a molecular simulation study, The Journal of Physical Chemistry B 116 (2012) 2259–2268.
[32] J.C. Phillips, R. Braun, W. Wang, J. Gumbart, E. Tajkhorshid, E. Villa, C. Chipot, R.D. Skeel, L. Kale, K. Schulten, Scalable molecular dynamics with NAMD, Journal of Computational Chemistry 26 (2005) 1781–1802.
[33] T.E. Cheatham, J.L. Miller, T. Fox, T.A. Darden, P.A. Kollman, Molecular dynamics simulations on solvated biomolecular systems: the particle mesh Ewald method leads to stable trajectories of DNA RNA, and proteins, Journal of the American Chemical Society 117 (1994) 4193–4194.
[34] J.P. Ryckaert, G. Ciccotti, H.J.C. Berendsen, Numerical integration of the cartesian equations of motion of a system with constraints: molecular dynamics of n-alkanes, Journal of Computational Physics 23 (1977) 327–341.
[35] M.J. Harvey, G. Giupponi, G. De Fabritiis, ACEMD: accelerating biomolecular dynamics in the microsecond time scale, Journal of Chemical Theory and Computation 5 (2009) 1632–1639.
[36] ACEMD. http://www.acellera.com/
[37] H.C. Andersen, RATTLE A: "Velocity" version of the SHAKE algorithm for molecular dynamics calculations, Journal of Computational Physics 52 (1983) 24–34.
[38] S.G. Lambrakos, J.P. Boris, E.S. Oran, I. Chandrasekhar, M. Nagumo, A modified SHAKE algorithm for maintaining rigid bonds in molecular dynamics simulations of large molecules, Journal of Computational Physics 85 (1989) 473–486.
[39] T. Giorgino, Gianni de Fabritiis, A high-throughput steered molecular dynamics study on the free energy profile of ion permeation through gramicidin A, Journal of Chemical Theory and Computation 7 (2011) 1943–1950.
[40] M. Selent, F. Sanz, M. Pastor, G. De Fabritiis, Induced effects of sodium ions on dopaminergic G-protein coupled receptors, PLOS Computational Biology 6 (2010) e1000884.
[41] I. Buch, T. Giorgino, G. De Fabritiis, Complete reconstruction of an enzyme-inhibitor binding process by molecular dynamics simulations, Proceedings of the National Academy of Science 108 (2011) 10184–10189.
[42] K.A. Feenstra, B. Hess, H.J.C. Berendsen, Improving efficiency of large time-scale molecular dynamics simulations of hydrogen-rich systems, Journal of Computational Chemistry 20 (1999) 786–798.
[43] W. Humphrey, A. Dalke, K. Schulten, VMD – visual molecular dynamics, Journal of Molecular Graphics 14 (1996) 33–38.
[44] E.F. Pettersen, T.D. Goddard, C.C. Huang, G.S. Couch, D.M. Greenblatt, E.C. Meng, T.E. Ferrin, UCSF Chimera – a visualization system for exploratory research and analysis, Journal of Computational Chemistry 25 (2004) 1605–1612.
[45] R. Lavery, M. Moakher, J.H. Maddocks, D. Petkeviciute, K. Zakrzewska, Conformational analysis of nucleic acids revisited: Curves+, Nucleic Acids Research 37 (2009) 5917–5929.
[46] M. Nowotny, S.A. Gaidamakov, R.J. Crouch, W. Yang, Crystal structures of RNase H bound to and RNA/DNA hybrid: substrate specificity and metal-dependent catalysis, Cell 121 (2005) 1005–1016.
[47] H. Wu, W.F. Lima, S.T. Crooke, Investigating the structure of human RNase H1 by site-directed mutagenesis, Journal of Biological Chemistry 276 (2001) 23547–23553.
[48] M. Nowotny, W. Yang, Stepwise analyses of metal ions in RNase H catalysis from substrate destabilization to product release, The EMBO Journal 25 (2006) 1924–1933.
[49] W.F. Lima, H. Wu, J.G. Nichols, H. Sun, H.M. Murray, S.T. Crooke, Binding and cleavage specificities of human argonaute 2, The Journal of Biological Chemistry 284 (2009) 26017–26028.
[50] D. M: Kenski, G. Butora, A.T. Willingham, A.J. Cooper, W. Fu, N. Qi, F. Soriano, I.W. Davies, W.M. Flanagan, siRNA-optimized modifications for enhanced in vivo Activity, Molecular Therapy – Nucleic Acids 1 (2012) e5.